Numerical Analysis of Nonuniform Geoelectric Field Impacts on Geomagnetic Induction in Pipeline Networks

Numerical Analysis of Nonuniform Geoelectric Field Impacts on Geomagnetic Induction in Pipeline Networks

Min-zhou Liu, *Graduate Student Member, IEEE,* Yan-zhao Xie, *Senior Member, IEEE,* Ning Dong, Zong-yang Wang, and Yi-fan Yang

***Abstract*—Modeling the geomagnetic induction in pipeline networks is essential for the risk assessment and management of geomagnetic disturbances. The induced geoelectric field (GEF) is usually spatially nonuniform, depending on the distribution of the geomagnetic variation and the earth conductivity. However, few studies have been conducted on the induction in complex pipeline networks with nonuniform GEF. In this paper, a calculation model for induction in pipeline networks with nonuniform GEF is proposed by utilizing the modified equivalent-pi circuits. Then the proposed model is used to investigate the distribution of pipe-to-soil potentials and geomagnetically induced currents in the pipeline network under several typical nonuniform GEF scenarios due to geomagnetic source fields, including local enhancement and spatially gradual variation. Furthermore, taking the coast effect as a typical case, the influence of the lateral variation of earth conductivity on the induction is analyzed. The results show that the nonuniform GEF may greatly affect the induction results in the local parts of the pipeline network.**

***Index Terms*—Geomagnetic disturbance, geomagnetically induced currents, nonuniform geoelectric field, pipe-to-soil potentials, pipeline network.**

I. Introduction

GEOMAGNETIC disturbances (GMD) caused by solar activities induce a low-frequency geoelectric field (GEF) on the earth's surface [1]–[3], thereby generating pipe-to-soil potentials (PSP) and geomagnetically induced currents (GIC) in the pipeline network. The geomagnetic induction may accelerate the corrosion of the pipeline, interfere with the cathodic protection system and other electrical equipment along the pipeline, which may have the potential to reduce the service life and even affect the operational safety of the pipeline [4]–[9]. Therefore, calculation of the geomagnetic induction in the pipeline is of great significance for evaluating the impacts of geomagnetic storms and identifying vulnerable pipes for protection.

This work was supported by National Key R&D Program of China under Grant 2016YFC0800100. *(Corresponding author: Yan-zhao Xie.)*

M.-z. Liu and N. Dong are with the State Key Laboratory of Electrical Insulation and Power Equipment, National Center for International Research on Transient Electromagnetics and Applications, School of Electrical Engineering, Xi'an Jiaotong University, Xi'an 710049, China, and also with the Department of Electronics and Telecommunications, Politecnico di Torino, 10129 Turin, Italy (e-mail: liuminzhou@outlook.com; dongning96@163.com).

Y.-z. Xie, Z.-y. Wang, and Y.-f. Yang are with the State Key Laboratory of Electrical Insulation and Power Equipment, National Center for International Research on Transient Electromagnetics and Applications, School of Electrical Engineering, Xi'an Jiaotong University, Xi'an 710049, China (e-mail: yzxie@mail.xjtu.edu.cn; wangzongyang@stu.xjtu.edu.cn; yangyf@stu.xjtu.edu.cn).

The induced GEF on the ground surface is usually spatially nonuniform, which is affected by the distribution of both the geomagnetic variation and the earth conductivity. For some types of GMD, such as auroral electrojet in the ionosphere at high latitudes, the space current system as an external source is relatively complex, and the resulting spatial distribution of magnetic field disturbances is less uniform than that at low latitudes [10]–[13]. Another cause of nonuniform GEF is the complex distribution of earth conductivity [14]–[20], especially the lateral variations in coasts, lakeshores, and geodetic fault zones, which may lead to a local GEF increase near the interface [20]–[22]. Some previous studies on GIC measurements and simulations have shown that the nonuniform GEF may greatly affect the induction results in the power grid [12], [14], [16], [17], whereas few studies exist on the nonuniform GEF induction in complex pipeline networks.

For the pipeline induction analysis, the transmission line model is usually required to obtain the PSP and GIC along the pipeline, which is different from the lumped circuit model used for GIC calculation in the power grid [1], [23], [24]. The interconnection of pipelines forms a complex network, which requires efficient induction algorithms for large-scale network analysis. Boteler and Cookson first proposed the distributed source transmission line (DSTL) model for geomagnetic induction in pipeline in 1986 [4]. Pulkkinen et al. adopted the equivalent Thevenin circuit model of the pipeline, and compared the induction results under different types of discontinuities such as the bends, junctions and branch points [5]. Boteler proposed the equivalent-pi circuit model of the pipeline under the *uniform* GEF in 2013, which is more suitable for the induction calculation of large-scale pipeline networks [6]. On the basis of the above studies, we propose a more general induction calculation model of pipeline networks under the spatially *nonuniform* GEF based on the transmission line theory, and study the influence of non-uniformity of GEF on PSP and GIC along the pipelines.

This paper is organized as follows. Section II briefly introduces the DSTL model of the geomagnetic induction in a pipeline with nonuniform GEF. Section III details the proposed equivalent-pi circuit model of pipeline under nonuniform GEF, and summarizes the algorithm of induction in pipeline networks. Then, the induction in the pipe network with nonuniform GEF caused by geomagnetic source field is analyzed in Section IV, and the results under local enhancement and gradual variations are compared. In Section V, the influence

of the lateral conductivity variation on the induction results is analyzed. Finally, Section VI presents the summary of this paper.

II. Geomagnetic Induction in a Pipeline With Nonuniform GEF

A. Modeling Nonuniform GEF

For the geomagnetic induction analysis of the pipe network and power grid, the induced horizontal electric field $\mathbf{E} = [E_x, E_y]^{\mathrm{T}}$ on the ground surface is required, which can be calculated by combining the horizontal magnetic field $\mathbf{B} = [B_x, B_y]^{\mathrm{T}}$ and the earth conductivity model. Their relationship at frequency f is as follows [1], [15]:

$$\mathbf{E}(f, \mathbf{x}) = \mathbf{K}(f, \mathbf{x}) \cdot \mathbf{B}(f, \mathbf{x}) \tag{1}$$

where $\mathbf{K}(f, \mathbf{x}) \in \mathbb{C}^{2\times 2}$ is the magnetotelluric transfer function (TF), also called magnetotelluric impedance in practical magnetotellurics [15], which can be inferred from electromagnetic measurements or numerical simulations; $\mathbf{x}$ is the spatial coordinates on the ground surface; and sub-x and sub-y refer to the components in the north and east directions.

The spatial distribution of the magnetic field can be calculated from the space source currents [1], [10], or obtained by spatial interpolation from the measurements at one or multiple geomagnetic observatories [13].

For the earth with 3-D complex distribution of conductivity, the response $\mathbf{K}(f, \mathbf{x})$ is usually a full matrix as in (2), and changes with the spatial coordinates [15]. In this case, the magnetic field and electric field on the earth surface are usually not orthogonal, thus resulting in a spatially nonuniform GEF.

$$\mathbf{K}(f, \mathbf{x}) = \begin{bmatrix} K_{xx} & K_{xy} \\ K_{yx} & K_{yy} \end{bmatrix} (f, \mathbf{x}) \tag{2}$$

For a uniform or 1-D horizontally layered earth model, the TF is reduced to (3), which can be calculated by the plane wave method [1].

$$\mathbf{K}(f, \mathbf{x}) = \begin{bmatrix} 0 & K \\ -K & 0 \end{bmatrix} (f, \mathbf{x}) \tag{3}$$

B. DSTL Model of Geomagnetic Induction in a Pipeline

To analyze the geomagnetic induction of the pipeline, we need to establish the transmission line model due to the weak conductivity of the external insulating coating of the pipeline in practice. Especially with the increase of service age, the conductivity of the coating may increase, and leakage points may even appear along the pipeline [25], [26].

In this section, the pipeline is represented as a 1-D transmission line along the x-axis for ease of expression. The DSTL model of the geomagnetic induction in a pipeline [5], [6] is shown in Fig. 1, where $E_{\mathrm{t}}(x)$ is the tangential component of the GEF along the pipeline, Z and Y are the series impedance and parallel admittance of the pipeline respectively, depending on the resistivity and geometric parameters of the steel and coating. In addition, the reactance and susceptance in the DSTL model are usually ignored because of the relatively low frequency of GMD (0.1 mHz-0.1 Hz).

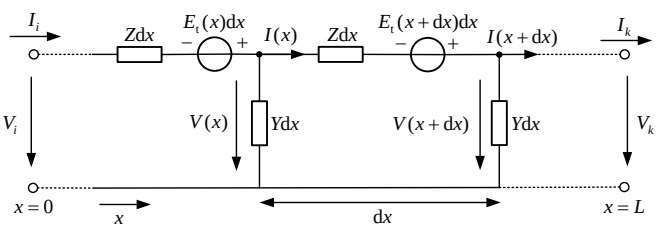

Fig. 1. Schematic diagram of DSTL model of geomagnetic induction in a pipeline with nonuniform GEF.

The propagation constant γ and characteristic impedance Z_{C} of the pipeline can be calculated as follows:

$$\gamma = \sqrt{ZY}, \quad Z_{\mathrm{C}} = \sqrt{Z/Y} \tag{4}$$

The transmission line equations of the pipeline under the external electric field are described as follows:

$$\begin{aligned} \frac{\mathrm{d}V(x)}{\mathrm{d}x} + ZI(x) &= E_{\mathrm{t}}(x) \\ \frac{\mathrm{d}I(x)}{\mathrm{d}x} + YV(x) &= 0 \end{aligned} \tag{5}$$

where V and I are the voltage and current along the pipeline, defined as PSP and GIC in pipeline induction, respectively.

Suppose the length of the pipe is L, and set the left end $x = 0$. The solution of the transmission line equations [27] is

$$\begin{bmatrix} V(x) \\ I(x) \end{bmatrix} = \mathbf{\Phi}(x) \begin{bmatrix} V(0) \\ I(0) \end{bmatrix} + \int_0^x \mathbf{\Phi}(x-z) \begin{bmatrix} E_{\mathrm{t}}(z) \\ 0 \end{bmatrix} \mathrm{d}z \tag{6}$$

where the chain-parameter matrix $\mathbf{\Phi}(x)$ of the pipeline is calculated by

$$\mathbf{\Phi}(x) = \begin{bmatrix} \cosh(\gamma x) & -Z_{\mathrm{C}} \sinh(\gamma x) \\ -\sinh(\gamma x)/Z_{\mathrm{C}} & \cosh(\gamma x) \end{bmatrix} \tag{7}$$

Thus, the relationship of the induced voltage and current between the two terminals of the pipeline (i, k) is as follows:

$$\begin{aligned} V_k =& \cosh(\gamma L) V_i - Z_{\mathrm{C}} \sinh(\gamma L) I_i \\ &+ \int_0^L \cosh\left(\gamma\left(L-z\right)\right) E_{\mathrm{t}}(z) \mathrm{d}z \end{aligned} \tag{8}$$

$$\begin{aligned} I_k =& -\frac{\sinh(\gamma L)}{Z_{\mathrm{C}}} V_i + \cosh(\gamma L) I_i \\ &- \int_0^L \frac{\sinh\left(\gamma(L-z)\right)}{Z_{\mathrm{C}}} E_{\mathrm{t}}(z) \mathrm{d}z \end{aligned} \tag{9}$$

where the convolution term is the equivalent source to characterize the effect of the GEF.

III. Calculation Model of Induction in Pipeline Networks With Nonuniform GEF

In this section, firstly the equivalent-pi circuit of the pipeline with a nonuniform GEF is established. Secondly, a nodal admittance matrix method for large-scale pipeline network analysis is proposed, and then the induced voltage and current along each pipeline can be obtained. Finally, the proposed algorithm is summarized and verified using a pipeline example.

The calculation formulas for the uniform GEF, as a special case, are listed in this section, and are consistent with the results in Reference [6].

A. Equivalent-Pi Circuit for Induction in a Pipeline

The pipeline excited by the induced GEF can be modeled as an equivalent-pi circuit. For discontinuities in the pipeline, such as bends, insulating flanges, leakage points, and branch points, additional nodes can be added to divide the pipeline into multiple segments, and the equivalent-pi circuit model is established for each segment.

Boteler proposed the equivalent-pi circuit model for the pipeline with uniform GEF $E_{\mathrm{t}}(x) = E_0$ [6], as shown in Fig. 2. The external uniform GEF is characterized by an equivalent current source I^E, which is computed as follows:

$$I^E = \frac{E_0}{Z} \tag{10}$$

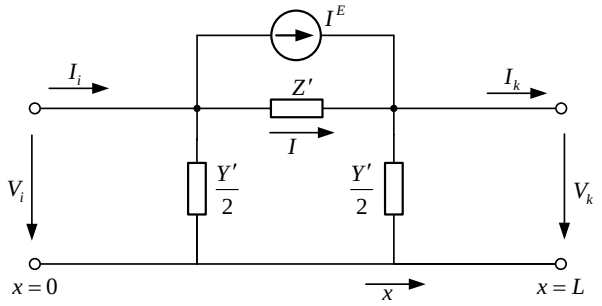

Fig. 2. Equivalent-pi circuit for induction in a pipeline with uniform GEF proposed by Boteler [6].

For the more general case of nonuniform GEF, we establish an equivalent-pi circuit with two equivalent current sources for the pipeline as depicted in Fig. 3, whose parameters are derived in detail below.

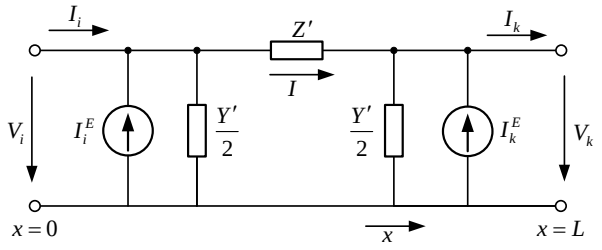

Fig. 3. Equivalent-pi circuit for induction in a pipeline with nonuniform GEF.

The relationship betweent the two ends of the equivalent-pi circuit in Fig. 3 can be obtained according to Kirchhoff's voltage and current laws:

$$\begin{aligned} V_k &= V_i - IZ' \\ I_i &= I + V_i\frac{Y'}{2} - I_i^E \\ I_k &= I - V_k\frac{Y'}{2} + I_k^E \end{aligned} \tag{11}$$

Thus, the voltage and current at node k can be expressed by those at node i as

$$V_k = \left(1 + \frac{Y'Z'}{2}\right) V_i - Z'I_i - Z'I_i^E \tag{12}$$

$$\begin{aligned} I_k = &- Y'\left(1 + \frac{Y'Z'}{4}\right) V_i + \left(1 + \frac{Y'Z'}{2}\right) I_i \\ &+ \left(1 + \frac{Y'Z'}{2}\right) I_i^E + I_k^E \end{aligned} \tag{13}$$

Comparing the coefficients in (12)-(13) with the results in (8)-(9) via transmission line theory, the parameters of the equivalent-pi circuit can be derived as

$$Z' = Z_{\mathrm{C}} \sinh \gamma L \tag{14a}$$

$$\frac{Y'}{2} = \frac{\cosh(\gamma L) - 1}{Z_{\mathrm{C}} \sinh \gamma L} \tag{14b}$$

$$I_i^E = -\frac{1}{Z_{\mathrm{C}} \sinh(\gamma L)} \int_0^L \cosh\left(\gamma(L - z)\right) E_{\mathrm{t}}(z) \mathrm{d}z \tag{14c}$$

$$I_k^E = \frac{1}{Z_{\mathrm{C}} \sinh(\gamma L)} \int_0^L \cosh\left(\gamma z\right) E_{\mathrm{t}}(z) \mathrm{d}z \tag{14d}$$

To calculate the equivalent current sources, different weights are given to the electric field along the line, hence the nonuniform electric field causes the difference in the amplitude of the two current sources. The effect of the nonuniform GEF depends on pipeline lengths: for an electrically short pipeline satisfying $L \ll 1/\gamma$ [5], we obtain $\cosh \gamma z \approx 1$ $(0 \le z \le L)$, thereby the influence of the non-uniformity of GEF is relatively small in this case; whereas the opposite is true for an electrically long pipeline.

In particular, for a uniform electric field $E_{\mathrm{t}}(x) = E_0$, the equivalent current sources in (14c)-(14d) can be simplified as

$$I_i^E = -\frac{E_0}{Z}, \quad I_k^E = \frac{E_0}{Z} \tag{15}$$

B. Calculating Nodal PSP via Admittance Matrix Method

The equivalent-pi circuits of pipelines are interconnected to form a network, as illustrated in Fig. 4, where the equivalent current sources on the connected pipelines are integrated into the nodal current injection.

The pipeline network is represented as an undirected graph $\mathcal{G} = (\mathcal{V}, \mathcal{E})$, where $\mathcal{V}$ is a set containing n_v vertices and $\mathcal{E}$ is a set containing n_e edges. The voltage of each node in the network can be calculated using the nodal admittance matrix method [1], [6]:

$$\mathbf{V} = \mathbf{Y}^{-1}\mathbf{J} \tag{16}$$

where $\mathbf{J} \in \mathbb{R}^{n_v \times 1}$ is the current source vector, and J_i is the sum of the equivalent current sources injected into node i via (17); $\mathbf{Y} \in \mathbb{R}^{n_v \times n_v}$ is the nodal admittance matrix, and the diagonal element Y_{ii} and the off-diagonal element Y_{ki} are calculated via (18).

$$J_i = \sum_{k \in i, k \neq i} j_{ik} \tag{17}$$

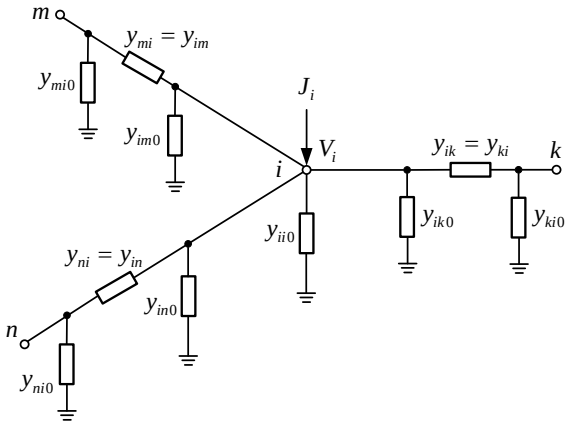

Fig. 4. Schematic diagram of the pipeline network, where node i is connected to node k, m, and n through pipelines.

where j_{ik} is the equivalent current source at node i of pipeline (i,k).

$$Y_{ii} = y_{ii0} + \sum_{k\in i, k\neq i} (y_{ik} + y_{ik0}), \quad Y_{ki} = -y_{ki} \tag{18}$$

where y_{ik} and y_{ik0} are parameters of the equivalent-pi circuit of pipeline (i,k) as depicted in Fig. 4, and y_{ii0} is the admittance of the additional grounding branch of node i.

C. Calculating PSP and GIC Along Pipelines

Different from the induction analysis in the power grid that regards the GIC along a line as an invariant, all PSP and GIC results along a line are usually required in the pipeline analysis, which can be solved by (19)-(20) based on the transmission line theory [5]. In addition, this step can be performed only on some pipelines of interest in the network.

$$V(x) = Z_{\mathrm{C}} \left((A + P(x))\, e^{-\gamma x} - (B + Q(x))\, e^{\gamma x} \right) \tag{19}$$

$$I(x) = (A + P(x))\, e^{-\gamma x} + (B + Q(x))\, e^{\gamma x} \tag{20}$$

where

$$\begin{aligned} P(x) &= \frac{1}{2Z_{\mathrm{C}}} \int_0^x e^{\gamma z} E_{\mathrm{t}}(z) \mathrm{d}z \\ Q(x) &= -\frac{1}{2Z_{\mathrm{C}}} \int_L^x e^{-\gamma z} E_{\mathrm{t}}(z) \mathrm{d}z \end{aligned} \tag{21}$$

The voltages at two terminals of the pipeline via the nodal admittance matrix method are used as boundary conditions:

$$\begin{aligned} V_i &= Z_{\mathrm{C}} \left(A - (B + Q(0)) \right) \\ V_k &= Z_{\mathrm{C}} \left((A + P(L))\, e^{-\gamma L} - B e^{\gamma L} \right) \end{aligned} \tag{22}$$

Thus, the coefficients of the general solution A and B can be calculated as follows:

$$\begin{aligned} A &= \frac{\left(V_k - V_i e^{\gamma L}\right)/Z_{\mathrm{C}} - P(L) e^{-\gamma L} - Q(0) e^{\gamma L}}{e^{-\gamma L} - e^{\gamma L}}, \\ B &= \frac{\left(V_k - V_i e^{-\gamma L}\right)/Z_{\mathrm{C}} - P(L) e^{-\gamma L} - Q(0) e^{-\gamma L}}{e^{-\gamma L} - e^{\gamma L}} \end{aligned} \tag{23}$$

Especially, for a uniform electric field, the voltage and current along the pipeline in (19)-(20) can be simplified into

$$V(x) = \frac{V_k - V_i e^{\gamma L}}{e^{-\gamma L} - e^{\gamma L}} e^{-\gamma x} - \frac{V_k - V_i e^{-\gamma L}}{e^{-\gamma L} - e^{\gamma L}} e^{\gamma x} \tag{24}$$

$$\begin{aligned} I(x) = &\frac{V_k - V_i e^{\gamma L}}{Z_{\mathrm{C}} \left(e^{-\gamma L} - e^{\gamma L}\right)} e^{-\gamma x} \\ &+ \frac{V_k - V_i e^{-\gamma L}}{Z_{\mathrm{C}} \left(e^{-\gamma L} - e^{\gamma L}\right)} e^{\gamma x} + \frac{E_0}{\gamma Z_{\mathrm{C}}} \end{aligned} \tag{25}$$

D. Procedure of Induction in Pipeline Network Algorithm

The detailed procedure to calculate the PSP and GIC in pipeline networks generated by the nonuniform induced GEF is shown in Algorithm 1.

Algorithm 1 Geomagnetic Induction in Pipeline Networks

Input: A pipeline network $\mathcal{G} = (\mathcal{V}, \mathcal{E})$ with topology, spatial coordinates of each node and transmission line parameters of each pipeline; spatial distribution of horizontal electric field vector $\mathbf{E}$.

Output: PSP and GIC of each pipeline.

1: **for** (i,k) in $\mathcal{E}$ **do**
2: Calculate the parameters of equivalent-pi circuit for pipeline (i,k) using (14a)-(14d);
3: **end for**
4: Make the nodal current injection vector $\mathbf{J}$ and the network admittance matrix $\mathbf{Y}$ as in (17)-(18);
5: Calculate the nodal PSP in the pipeline network via (16);
6: **for** (i,k) in $\mathcal{E}$ **do**
7: Calculate the induced voltage and current along the pipeline (i,k) via (19)-(20);
8: **end for**

For a uniform GEF, the simplified (15) can be used to calculate the current sources in the equivalent-pi circuit, and (24)-(25) can be used to calculate the PSP and GIC along the pipeline instead.

For an actual pipeline network on the 2-D ground surface given the nodal coordinates, the 1-D line integrals of the tangential electric field in the above equations need to be extended to the 2-D line integrals of the electric field vector. The line integrals along the pipeline (i,k) of the product of a certain function $g(\mathbf{x})$ and the GEF can be calculated as follows:

$$\begin{aligned} \int_{\mathbf{x}_i}^{\mathbf{x}_k} g(\mathbf{x}) \mathbf{E}(\mathbf{x}) \mathrm{d}\mathbf{l} = &\int_{\mathbf{x}_i}^{\mathbf{x}_k} g(\mathbf{x}) E_x(\mathbf{x}) \mathrm{d}x \\ &+ \int_{\mathbf{x}_i}^{\mathbf{x}_k} g(\mathbf{x}) E_y(\mathbf{x}) \mathrm{d}y \end{aligned} \tag{26}$$

where $\mathrm{d}x$ and $\mathrm{d}y$ represent the northward and eastward lengths of $\mathrm{d}\mathbf{l}$ respectively, which can be calculated via Reference [28] if nodal coordinates are expressed in latitude and longitude.

E. Verification of Induction Algorithm With Nonuniform GEF

A single northward pipeline with insulated ends is used to validate the induction algorithm for nonuniform GEF. The pipeline length is 500 km. The series impedance Z is 0.005 Ω/km, and the parallel admittance Y is 0.05 S/km. The above parameters are from a typical case of electrically long pipes in [5], since the nonuniform GEF has a relatively greater effect on electrically long pipes as discussed in Section III-A. The

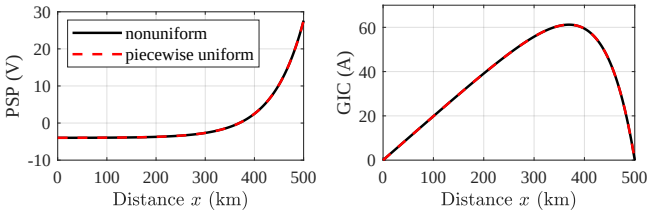

(a) PSP along pipeline (b) GIC along pipeline

Fig. 5. Comparison of PSP and GIC results with respect to distance x along the pipeline using nonuniform and piecewise uniform algorithms.

spatial distribution of the nonuniform GEF is assumed to be $E_{\mathrm{t}}(x) = 0.001x$ V/km, where x is the distance along the pipeline in kilometers.

The induction algorithms in this paper are implemented in MATLAB R2019b. The following two methods are used for comparison: 1) Nonuniform method: an equivalent-pi circuit model with nonuniform GEF is established via (14a)-(14d), resulting in a 2-node network; 2) Piecewise uniform method: the pipeline is equally divided into 500 sections by length, and the GEF of each segment is taken as the value located at the midpoint. An equivalent-pi circuit model with uniform GEF is established for each segment using (10), resulting in a network of 501 nodes. The PSP and GIC along the pipeline obtained by the two methods are highly consistent, as shown in Fig. 5, which illustrates the accuracy of the proposed model. In addition, the former method can reduce the order of the nodal admittance matrix in (16) by simplifying each pipeline into an equivalent circuit, thereby decreasing the computational burden.

IV. Effects of Nonuniform Geomagnetic Source Fields on Induction in Pipeline Networks

A. Locally Enhanced and Gradually Changing Nonuniform GEF Scenarios

The spatial distribution of the nonuniform GEF used in this section is from the EPRI report [12], provided in a $0.5^\circ \times 0.5^\circ$ regular grid, which includes two scenarios visualized in Fig. 6. In scenario 1, there is a local enhancement in the GEF magnitude to 12 V/km in an area of $1^\circ \times 1^\circ$, while the remaining area is 1.2 V/km, and the GEF direction is modified to east in this paper. This type of GEF is caused by the local enhancement of the geomagnetic field occurring in areas of hundreds of kilometers at high latitudes, rather than the lateral changes in earth conductivity [11]. In scenario 2, both the magnitude and direction of the GEF vary gradually with the spatial coordinates. The spatial distribution of space currents at high latitudes is quite complicated, and the above two scenarios are regarded as typical GEF caused by nonuniform geomagnetic source fields in this paper.

B. Synthetic Test Pipeline Network 1

A modified 9-node and 8-line test pipeline network presented in Fig. 7 is used for induction analysis in this section, whose spatial cooridnates are listed in Appendix Table A-I, including a main line '3-4-5-6-7-8' and three branch lines '1-3', '2-3' and '7-9'. The original data are obtained from Boteler's paper [6], and some parameters have been adjusted. The length of each pipeline has been modified into twice the original length to match the footprint of the GEF in this section. The series resistance of the main and branch pipeline is 0.00492 and 0.01544 Ω/km, and the parallel conductance is 0.012 and 0.006 S/km, respectively.

C. Induction Results With Nonuniform GEF

For the two nonuniform GEF scenarios, the induction results in the pipe network are compared with the corresponding uniform GEF. The nodal PSP and maximum line GIC are shown in Table I and Table II, and the PSP and GIC along the main pipeline 3-8 are shown in Fig. 8.

If we compare the induction results of nonuniform GEF scenario 1 with those of 1.2 V/km eastward uniform base case, we can see that the PSP of almost all nodes and the maximum GIC of all pipelines in the network have increased significantly due to local GEF enhancement. The spatially locally enhanced GEF covers all of the pipeline 4-5 and a part of the pipeline 3-4 and 5-6. The induction results of these pipelines are directly affected by the nonuniform GEF, while the changes in the results of other pipelines are mainly caused by network interconnection.

In the case of a uniform GEF, the peak of PSP is at the end of the main pipe, which is called the corner effect, while the peak of GIC appears in the middle of the pipe. After the GEF is locally enhanced, the PSP peak appears at the edge of the GEF enhanced area, and the GIC increse of the pipeline located in the GEF enhanced area is higher than that of other pipelines.

For the nonuniform GEF scenario 2, the spatial distribution of the GEF amplitude is characterized by being smaller in the west and larger in the east. As a comparison, the uniform GEF case is taken as the average value of scenario 2, resulting in a southeast GEF of $E_x = -0.945$ V/km, $E_y = 4.337$ V/km. The induction results along the main pipeline under nonuniform and uniform GEF are compared in Fig. 8. It can be seen that the overall spatial distributions of PSP and GIC are similar in the two cases, but there is a deviation in amplitude. The spatial averaging of the GEF leads to an underestimation of the PSP and GIC magnitudes in the east of the network, corresponding to the area with a larger local GEF, whereas the induction results are overestimated in the area with a smaller local GEF.

V. Effects of Lateral Conductivity Variations on Induction in Pipeline Networks

A. Nonuniform GEF Due to Lateral Conductivity Variations

The lateral variation of the earth conductivity causes the distortion of the GEF near the interface, which affects the induction results in pipeline networks. Fig. 9 presents the thin-sheet coast model from Reference [20] adopted for demonstration. The parameters in the model are set as follows: The space source current is a uniform surface current at 100 km in height, with an amplitude of 1 A/m and a cosine waveform at 0.001 Hz; the depths of sea and land are 5 km and 500 km,

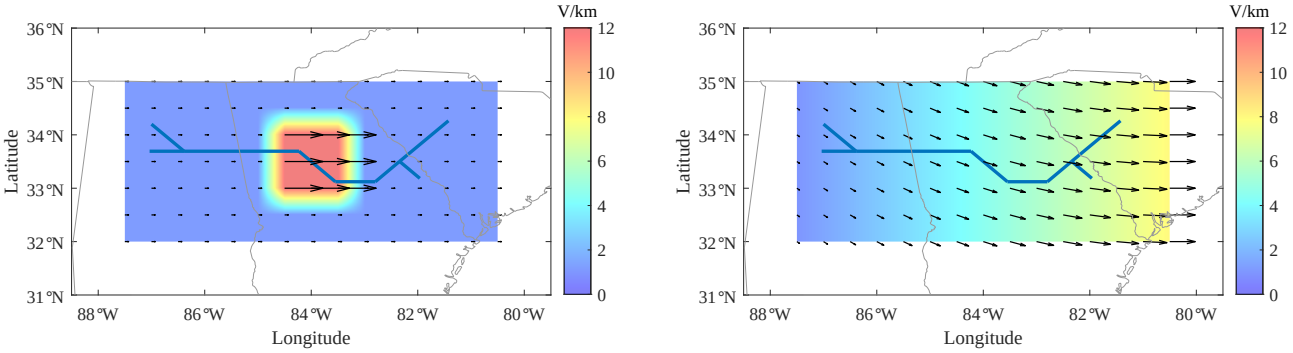

(a) Scenario 1: Eastward local enhancement

(b) Scenario 2: Southeast GEF

Fig. 6. Spatial distribution of the nonuniform GEF. The arrow in the figure indicates the electric field vector from the EPRI report [12]; the colored map visualizes the spatial distribution of the interpolated GEF; the blue line shows the location of the pipes, and the gray curve is the base map.

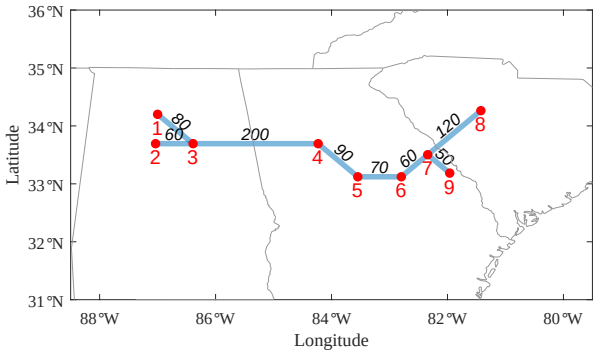

Fig. 7. The synthetic 9-node and 8-pipeline network 1. The red labels indicate the number of nodes, and the black labels are pipeline lengths in kilometers.

TABLE I
NODAL PSP (V) IN PIPELINE NETWORK 1*

Node	GEF Scenario 1		GEF Scenario 2	
	Nonuniform	Uniform	Nonuniform	Uniform
1	-266.76	-124.84	-297.46	-495.81
2	-299.47	-140.62	-284.65	-508.07
3	-274.63	-88.61	-236.49	-320.09
4	-104.01	4.86	-87.45	3.61
5	228.72	5.93	-7.83	57.37
6	345.66	34.40	130.34	161.00
7	246.97	44.77	165.08	166.21
8	250.29	111.31	504.54	342.27
9	260.46	79.56	384.28	322.46

* The gray cell indicates that the node is located in the local enhancement area of the GEF.

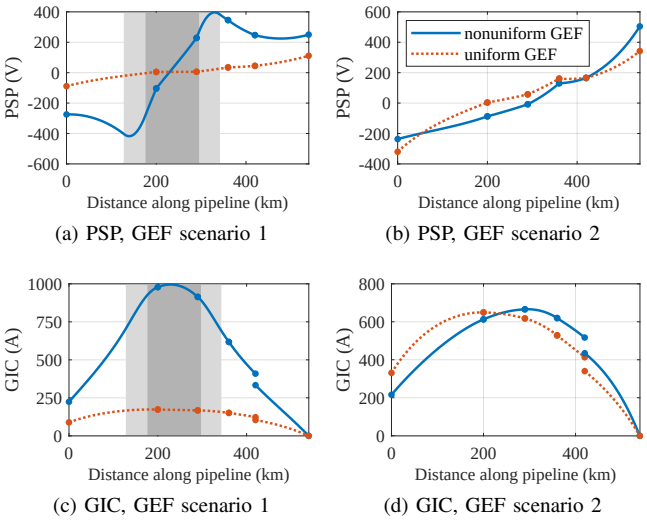

(a) PSP, GEF scenario 1

(b) PSP, GEF scenario 2

(c) GIC, GEF scenario 1

(d) GIC, GEF scenario 2

Fig. 8. Comparison of PSP and GIC results with distance along the main pipeline '3-8' of network 1 in the case of nonuniform and uniform GEF. The points in the figure indicate the positions of nodes along the main pipeline. (In subfigure (a) and (c), the dark gray part of the pipeline is located in the 12 V/km enhanced area, the white part is located in the 1.2 V/km base area, and the light gray part is located in the linear transition area from 12 V/km to 1.2 V/km.)

TABLE II
MAXIMUM LINE GIC (A) IN NETWORK 1*

From Node	To Node	GEF Scenario 1		GEF Scenario 2	
		Nonuniform	Uniform	Nonuniform	Uniform
3	4	979.27	173.49	613.02	649.59
4	5	995.50	173.07	665.63	649.26
5	6	914.65	167.49	666.27	617.93
6	7	617.87	150.90	619.45	528.45
7	8	333.41	104.35	434.52	340.14
1	3	123.42	48.57	123.25	185.57
2	3	100.31	40.05	92.10	144.70
7	9	74.39	18.15	79.83	71.30

* The gray cell indicates that part or all of the pipeline is located in the local enhancement area of the GEF.

and the conductivity is 4 S/m and 0.01 S/m, respectively. The finite element method [19], [20], [22] is used to calculate the spatial distribution of the induced GEF on the earth surface, and the block model is used as a comparison to illustrate the additional influence of ocean, i.e., the GEFs on the surface of land and sea are calculated separately by the plane wave method without considering their mutual influence [1], [14].

The direction of the space source currents is taken as east and north respectively, and the resulting surface GEF distribu-

tion is shown in Fig. 10. In the two cases, the GEFs near the interface show different changes. For the space source currents perpendicular to the coast, i.e., along the east direction, an eastward GEF is induced on the earth surface, and the H-polarization [20] causes the GEF to increase on the land side near the interface. For the space source currents parallel to the coast, a northward GEF is induced on the earth surface, and the E-polarization [19] causes the GEF distortion, whose changes are opposite to the H-polarization case.

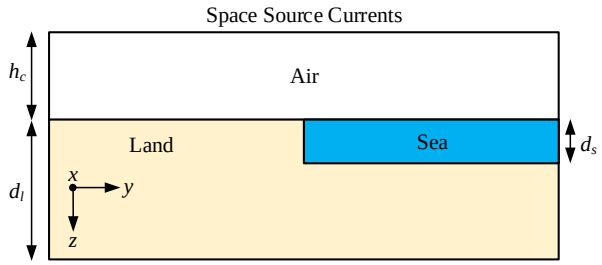

Fig. 9. Schematic diagram of coast model excited by space source currents. The earth surface is on the $z = 0$ plane, and the coast is along the north direction at $y = 0$. The height of the space source currents, the depth of the ocean and land are h_c, d_s and d_l, respectively.

B. Induction Results Considering Coast Effect

This section adopts the synthetic test pipe network 2 from Reference [6] for induction analysis, as shown in Fig. 11, and the nodal coordinates are detailed in Appendix Table A-I. The GEF results obtained by the thin-sheet model and the block model, denoted as E_{3D} and E_{1D}, are used as inputs to analyze the induction in the pipe network. Due to the phase difference between the GEF at different locations on the surface, the real and imaginary parts of the GEF are used for the induction calculation separately, which are then combined to obtain the final amplitudes of the PSP and GIC in the pipelines.

The PSP along the main pipeline is shown in Fig. 12. The PSP of node 8 near the coast is analyzed as an example: for H-polarization, due to coast effect, the PSP of node 8 increases to 138.0% of that in the case of 1-D uniform land; whereas for E-polarization, it decreases to 33.8% of the original. The induction results of other pipes have relatively small changes due to the larger distance from the coast.

C. Influence of Coast at Different Frequencies

The influence of coast at different frequencies on the induction in the pipe network is analyzed. The ratio of GEF on the land side near the coast obtained by thin-sheet model and block model E_{3D}/E_{1D} is used to illustrate the extent of the coast effect. As shown in Fig. 13, with the frequency increases, the enhancement effect of the H-polarization on the GEF gradually decreases, whereas the weakening effect of the E-polarization on the GEF tends to grow gradually stronger.

The effective distances of the coast effect, defined as the distance from the coast within which the difference between E_{3D} and E_{1D} on the land is greater than 10% [20], at different frequencies are shown in Fig 14. The effective distance of the

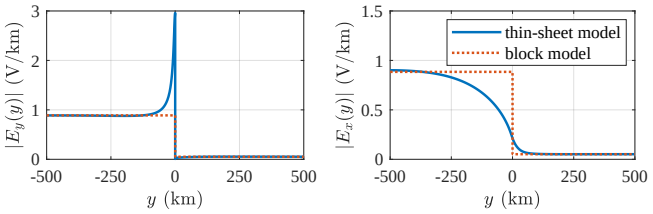

(a) GEF, H-polarization (b) GEF, E-polarization

Fig. 10. Comparison of GEF at 0.001 Hz based on thin-sheet and block earth model.

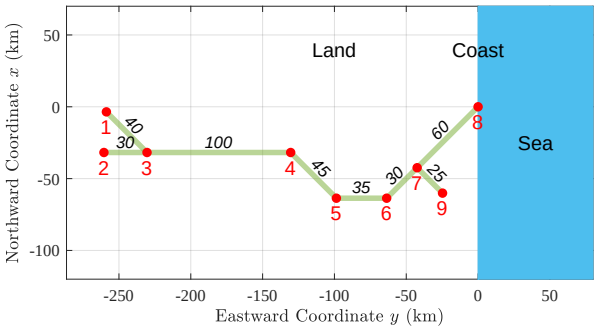

Fig. 11. The synthetic 9-node and 8-pipeline network 2. The red labels indicate the number of nodes, and the black labels are pipeline lengths in kilometers.

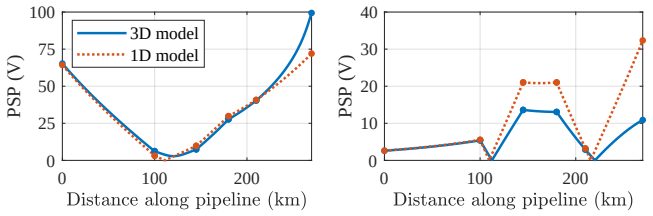

(a) PSP, H-polarization (b) PSP, E-polarization

Fig. 12. Comparison of PSP with distance along the main pipeline 3-8 of network 2 at 0.001 Hz in the case of 3-D and 1-D earth model.

E-polarization is larger than that of the H-polarization, and both generally tend to decrease as the frequency increases.

Correspondingly, the PSP of node 8 using thin-sheet and block model, denoted by PSP_{3D} and PSP_{1D}, is presented in Fig. 15. The change of the PSP magnitude in percentage is smaller than that of the GEF, since the coast effect weakens as the distance from the coast increases. As the frequency increases, the enhancement effect of H-polarization on the PSP amplitude gradually weakens, which is consistent with the GEF change shown in Fig. 13a; whereas for E-polarization, the weakening of the PSP amplitude is slight at higher frequencies, which is different from the GEF change depicted in Fig. 13b, mainly due to the shorter effective distance of the coast effect at higher frequencies. The above results are similar to the impact of the coast on GICs in the power grid [19], [20]. In summary, for the pipe network example presented, the coast affects the PSP of node 8 more at lower frequencies (10^{-4} Hz-10^{-3} Hz), regardless of H-polarization or E-polarization.

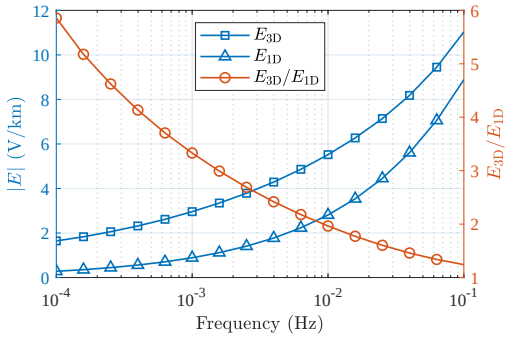

(a) GEF, H-polarization

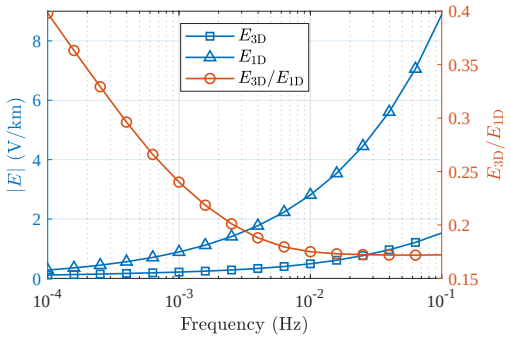

(b) GEF, E-polarization

Fig. 13. Comparison of GEF results on the land side near the coast using 3-D and 1-D earth model with respect to the frequencies.

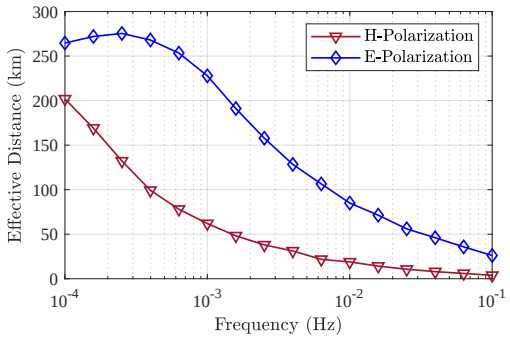

Fig. 14. Effective distance of coast effect at different frequencies.

D. Effects of GEF Spatial Distribution on Inductions in Pipeline Networks Using Measured Magnetotelluric Responses

The regional GEF is usually spatially averaged due to the lack of magnetotelluric measurements or the simplification of induction simulation models [1], [29], [30]. This section analyzes its influence on the induction results in pipeline networks based on EMTF data measured near an actual coast.

The EMTF data at 1,112 USArray sites were obtained from the IRIS Data Services website [31]. The geomagnetic time series at the Ottawa (OTT) observatory from NRCan [32] during March 13-14, 1989 was selected to calculate the GEF. The calculation process of the GEF spatial distribution is as follows: first calculate the GEF waveform at each EMTF site, and then perform spatial smoothing, i.e., the updated GEF result at each site is the average value at the sites within

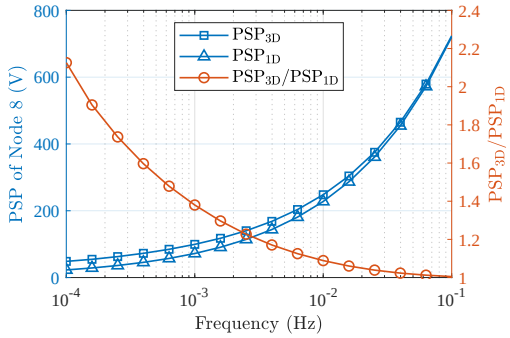

(a) PSP of node 8, H-polarization

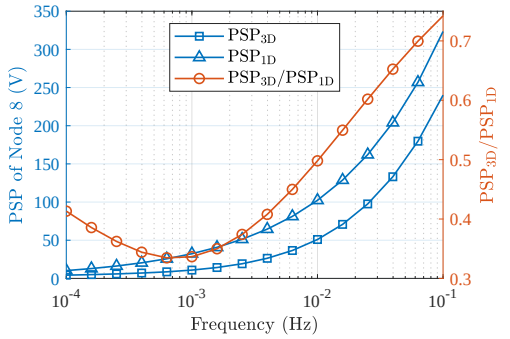

(b) PSP of node 8, E-polarization

Fig. 15. Comparison of PSP of node 8 using 3-D and 1-D earth model with respect to the frequencies.

a given distance, finally the GEF is scaled according to the geomagnetic latitude of each site via (27). For GMD risk assessment, the empirical formula (27) can be used to scale the GEF to characterize the intensity of geomagnetic activities at different geomagnetic latitudes [11].

$$\alpha(\lambda) = \begin{cases} 0.1, & \text{if } \lambda \le 40^\circ \\ 0.001 \times e^{0.115\lambda}, & \text{if } 40^\circ<\lambda<60^\circ \\ 1, & \text{if } \lambda \ge 60^\circ \end{cases} \tag{27}$$

where λ is the geomagnetic latitude in degrees.

A GEF peak at 1:17 on March 14, 1989 is selected for the induction analysis of the pipeline network. The spatial distributions of original GEF at the EMTF sites and the GEF under different smoothing distances are shown in Fig. 16. Spatial smoothing weakens the sharp peak of the GEF and also causes the loss of local details of the GEF spatial distribution.

This section adopts another modification of the synthetic pipeline network from Reference [6], denoted as network 3. Network 3 is obtained by spatial translation of network 1 maintaining the pipe lengths. The geographic coordinate of node 1 in network 3 is (41°N, 81°W), and the pipe network passes through the GEF enhancement area on the east coast. All nodes in the test network 3 are located within the envelope of the EMTF sites in order to avoid spatial extrapolation of the GEF.

EMTF sites are usually scattered points with irregular spatial distribution. In this respect, in the pipeline induction calculation, the GEF vector along the pipeline is obtained by interpolation of the value at the EMTF sites based on the Delaunay triangulation [17].

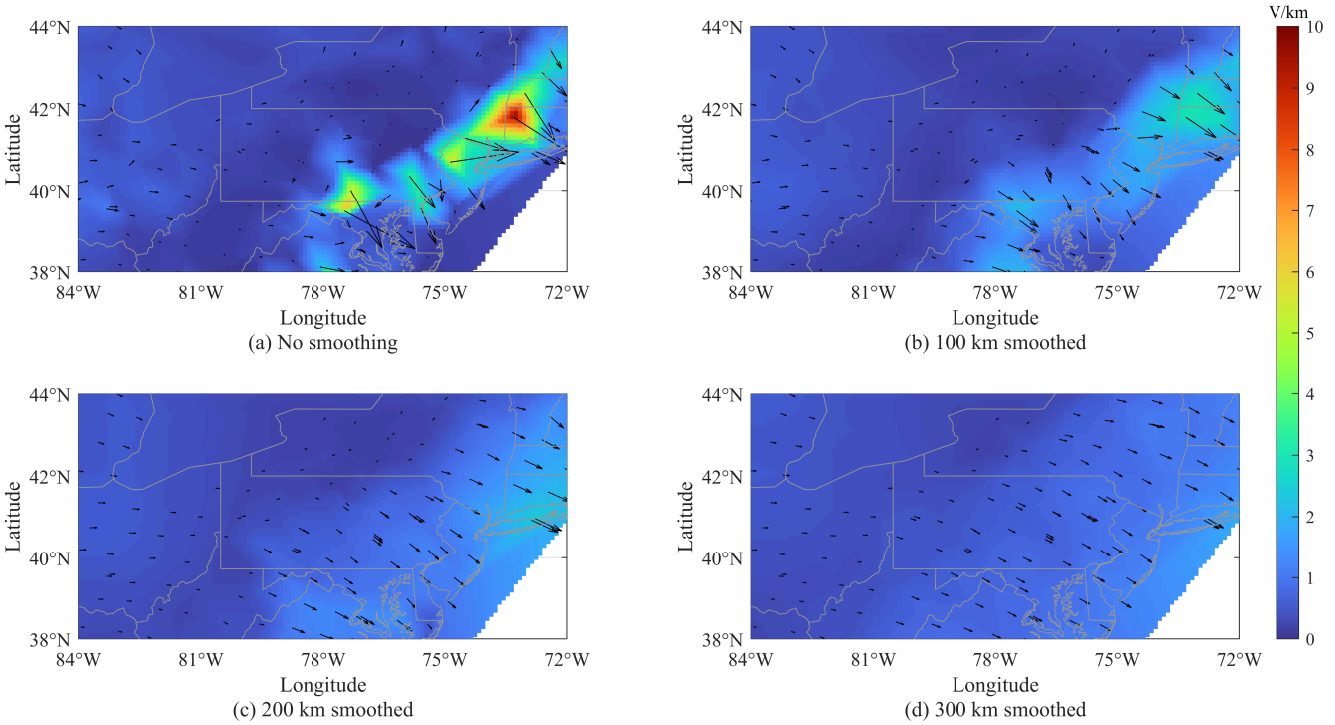

Fig. 16. Snapshots of the simulated GEF spatial distribution on the east coast under different spatial smoothing distances at 1989-03-14 01:17. The arrow in the figure indicates the GEF vector at the EMTF sites [31]; the color map visualizes the spatial distribution of linear interpolated GEF; and the gray curve is the base map.

First, we compare the induction results along the main pipeline of network 3 under GEF smoothing at different distances, where the GEF is linearly interpolated along each pipeline. As shown in Fig. 17, as the smoothing distance increases, the peak PSP and GIC amplitudes of the pipeline tend to decrease. The GEF spatial averaging may smooth out the fluctuating details of the induction results along the line, causing some risky sections of the pipeline to be unrecognizable.

In addition, the influence of different interpolation methods of GEF on the induction of pipe network is analyzed. The original GEFs at the EMTF sites are interpolated along the pipeline using linear, nearest neighbor, and natural neighbor interpolation methods [33], respectively. Fig. 18 shows the difference in pipeline induction results using different interpolation methods, where nearest neighbor interpolation method yields larger values. Hence, the modeling and measurement of GEFs at finer spatial granularity are important for accurate assessment of geomagnetic induction in pipeline networks.

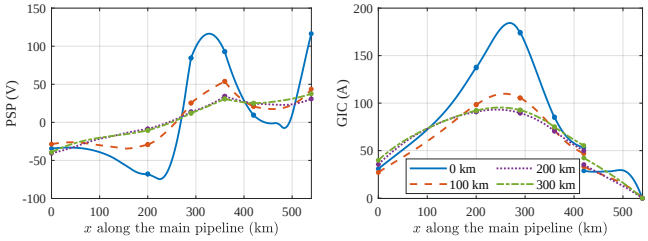

(a) PSP along the main pipeline (b) GIC along the main pipeline

Fig. 17. Comparison of PSP and GIC results along the main pipeline of network 3 in the cases of different spatial smoothing distances.

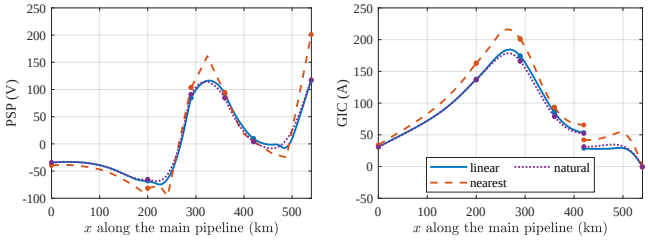

(a) PSP along the main pipeline (b) GIC along the main pipeline

Fig. 18. Comparison of PSP and GIC results along the main pipeline of network 3 in the cases of linear, nearest neighbor and natural neighbor interpolation of GEFs.

VI. Conclusions

In this paper, we propose a calculation method for the geomagnetic induction in pipeline networks with nonuniform GEF. The influence of the typical nonuniform GEF distribution due to geomagnetic source fields such as local enhancement and gradual variation on the induction results in the pipe network is investigated, which shows that there is a relatively large difference in PSP and GIC compared with uniform GEF. In addition, the lateral conductivity variations also have a great impact on induction in pipe networks, especially at low frequencies, and H-polarization and E-polarization cause increase and decrease of the PSP near the interface, respec-

tively. Moreover, using the induction results in the pipeline network based on magnetotelluric response measurements, the influence of the spatial smoothing and interpolation method of the GEF on the pipeline induction is analyzed. The model proposed in this paper can be used to evaluate the geomagnetic induction in pipelines passing through complex geology if GEF distribution with finer spatial granularity is available.

APPENDIX

The nodal spatial coordinates of the synthetic modified 9-node and 8-line networks are shown in Table A-I.

TABLE A-I
NODAL COORDINATES OF SYNTHETIC TEST PIPELINE NETWORKS*

Node	Network 1**		Network 2	
	Latitude (°N)	Longitude (°E)	x (km)	y (km)
1	34.200	-87.000	-3.536	-258.744
2	33.693	-87.035	-31.820	-260.460
3	33.693	-86.388	-31.820	-230.460
4	33.693	-84.231	-31.820	-130.460
5	33.122	-83.547	-63.640	-98.640
6	33.122	-82.797	-63.640	-63.640
7	33.503	-82.341	-42.426	-42.426
8	34.263	-81.424	0	0
9	33.185	-81.961	-60.104	-24.749

* The spatial coordinates of network 1 and network 2 are expressed in latitude-longitude and distance, respectively.
** The pipeline lengths in network 1 are changed into twice the original data from Reference [6].

ACKNOWLEDGMENT

We gratefully acknowledge the Natural Resources Canada (NRCan) in providing the geomagnetic data at OTT observatory. The work was supported by the Outstanding Chinese and Foreign Youth Exchange Program of China Association for Science and Technology (CAST), and also supported by the HPC platform at Xi'an Jiaotong University.

REFERENCES

[1] D. Boteler and R. Pirjola, "Modeling geomagnetically induced currents," *Space Weather*, vol. 15, no. 1, pp. 258–276, 2017.
[2] A. Pulkkinen *et al.*, "Geomagnetically induced currents: Science, engineering, and applications readiness," *Space Weather*, vol. 15, no. 7, pp. 828–856, 2017.
[3] J. Kappenman, "Geomagnetic storms and their impacts on the US power grid," Metatech Corporation, Goleta, CA, Tech. Rep. Meta-R-319, 2010.
[4] D. Boteler and M. Cookson, "Telluric currents and their effects on pipelines in the cook strait region of New-Zealand," *Mater. Perform.*, vol. 25, no. 3, pp. 27–32, 1986.
[5] A. Pulkkinen, R. Pirjola, D. Boteler, A. Viljanen, and I. Yegorov, "Modelling of space weather effects on pipelines," *J. Appl. Geophys.*, vol. 48, no. 4, pp. 233–256, 2001.
[6] D. Boteler, "A new versatile method for modelling geomagnetic induction in pipelines," *Geophys. J. Int.*, vol. 193, no. 1, pp. 98–109, 2013.
[7] P. A. Fernberg, C. Samson, D. H. Boteler, L. Trichtchenko, and P. Larocca, "Earth conductivity structures and their effects on geomagnetic induction in pipelines," *Ann. Geophys.*, vol. 25, no. 1, pp. 207–218, 2007.
[8] Z. Yu, J. Hao, L. Liu, and Z. Wang, "Monitoring experiment of electromagnetic interference effects caused by geomagnetic storms on buried pipelines in China," *IEEE Access*, vol. 7, pp. 14 603–14 610, 2019.
[9] D. Boteler, "Geomagnetic effects on the pipe-to-soil potentials of a continental pipeline," *Adv. Space Res.*, vol. 26, no. 1, pp. 15–20, 2000.
[10] K. Zheng, R. J. Pirjola, D. H. Boteler, and L.-g. Liu, "Geoelectric fields due to small-scale and large-scale source currents," *IEEE Trans. Power Del.*, vol. 28, no. 1, pp. 442–449, Jan. 2013.
[11] *Transmission system planned performance for geomagnetic disturbance events*, North American Electric Reliability Corporation (NERC) Std. TPL-007-2, Oct. 2017.
[12] "Geomagnetic disturbance (GMD) non-uniform field benchmark test case: Benchmarking geomagnetically induced currents with non-uniform geoelectric fields," Electr. Power Res. Inst., Palo Alto, CA, Tech. Rep. 3002018766, 2020.
[13] O. Amm and A. Viljanen, "Ionospheric disturbance magnetic field continuation from the ground to the ionosphere using spherical elementary current systems," *Earth, Planets and Space*, vol. 51, no. 6, pp. 431–440, 1999.
[14] L. Marti, C. Yiu, A. Rezaei-Zare, and D. Boteler, "Simulation of geomagnetically induced currents with piecewise layered-earth models," *IEEE Trans. Power Del.*, vol. 29, no. 4, pp. 1886–1893, Aug. 2014.
[15] A. Kelbert, C. C. Balch, A. Pulkkinen, G. D. Egbert, J. J. Love, E. J. Rigler, and I. Fujii, "Methodology for time-domain estimation of storm time geoelectric fields using the 3-D magnetotelluric response tensors," *Space Weather*, vol. 15, no. 7, pp. 874–894, 2017.
[16] A. Kelbert, "The role of global/regional earth conductivity models in natural geomagnetic hazard mitigation," *Surv. Geophys.*, vol. 41, no. 1, pp. 115–166, 2020.
[17] R. Sun and C. Balch, "Comparison between 1-D and 3-D geoelectric field methods to calculate geomagnetically induced currents: A case study," *IEEE Trans. Power Del.*, vol. 34, no. 6, pp. 2163–2172, Dec. 2019.
[18] Y.-h. Chen, Y.-z. Xie, M.-z. Liu, Z.-y. Wang, Q. Liu, and A.-c. Qiu, "Geomagnetically induced current calculation of high voltage power system with long transmission lines using Kriging method," *IEEE Trans. Power Del.*, vol. 37, no. 1, pp. 650–657, 2022.
[19] C. Liu, X. Wang, C. Lin, and J. Song, "Proximity effects of lateral conductivity variations on geomagnetically induced electric fields," *IEEE Access*, vol. 7, pp. 6240–6248, 2019.
[20] C. Liu, X. Wang, S. Zhang, and C. Xie, "Effects of lateral conductivity variations on geomagnetically induced currents: H-polarization," *IEEE Access*, vol. 7, pp. 6310–6318, 2019.
[21] J. L. Gilbert, "Simplified techniques for treating the ocean–land interface for geomagnetically induced electric fields," *IEEE Trans. Electromagn. Compat.*, vol. 57, no. 4, pp. 688–692, Aug. 2015.
[22] H. Karami, K. Sheshyekani, A. Rezaei-Zare, and J. Mahseredjian, "Effect of mixed propagation path on electromagnetic fields at ground surface produced by electrojet," *IEEE Trans. Electromagn. Compat.*, vol. 60, no. 6, pp. 2019–2024, Dec. 2018.
[23] K. Zheng, D. Boteler, R. J. Pirjola, L.-g. Liu, R. Becker, L. Marti, S. Boutilier, and S. Guillon, "Effects of system characteristics on geomagnetically induced currents," *IEEE Trans. Power Del.*, vol. 29, no. 2, pp. 890–898, Apr. 2014.
[24] Q. Liu, Y.-z. Xie, N. Dong, Y.-h. Chen, M.-z. Liu, and Q. Li, "Uncertainty quantification of geo-magnetically induced currents in UHV power grid," *IEEE Trans. Electromagn. Compat.*, vol. 62, no. 1, pp. 258–265, Feb. 2020.
[25] B. Zhang, F. Cao, R. Zeng, J. He, X. Meng, Y. Liao, and R. Li, "DC current distribution in both AC power grids and pipelines near HVDC grounding electrode considering their interaction," *IEEE Trans. Power Del.*, vol. 34, no. 6, pp. 2240–2247, Dec. 2019.
[26] C. Ma and C. Liu, "Influence of pipeline insulation leakage points on the distribution of geomagnetically induced current and pipe-soil potential," *IEEE Access*, vol. 7, pp. 147 470–147 480, 2019.
[27] C. R. Paul, "Incident field excitation of two-conductor line," in *Analysis of Multiconductor Transmission Lines*, 2nd ed. Hoboken, NJ: John Wiley & Sons, Inc., 2008, ch. 11, pp. 578–592.
[28] R. Horton, D. Boteler, T. J. Overbye, R. Pirjola, and R. C. Dugan, "A test case for the calculation of geomagnetically induced currents," *IEEE Trans. Power Del.*, vol. 27, no. 4, pp. 2368–2373, Oct. 2012.
[29] "Improving conductivity models for geomagnetically induced current (GIC) estimation: Guidance for validation of GIC models," Electr. Power Res. Inst., Palo Alto, CA, Tech. Rep. 3002017897, 2020.
[30] "Use of magnetotelluric measurement data to validate/improve existing earth conductivity models," Electr. Power Res. Inst., Palo Alto, CA, Tech. Rep. 3002019425, 2020.
[31] A. Kelbert, G. Egbert, and A. Schultz, "IRIS DMC data services products: EMTF, the magnetotelluric transfer functions," 2011, https://doi.org/10.17611/DP/EMTF.1. Accessed on: Jul. 24, 2021.

[32] "Magnetic data," Natural Resources Canada, https://geomag.nrcan.gc.ca/. Accessed on: Jun. 9, 2021.
[33] I. Amidror, "Scattered data interpolation methods for electronic imaging systems: a survey," *J. Electron. Imaging*, vol. 11, no. 2, pp. 157–176, 2002.

Min-zhou Liu (Graduate Student Member, IEEE) was born in Hebei, China, in 1995. He received the B.S. degree in electrical engineering from Xi'an Jiaotong University, Xi'an, China, in 2017. He is currently pursing the Ph.D. degree in electrical engineering under the double degree program jointly supported by Xi'an Jiaotong University and Politecnico di Torino, Turin, Italy.

His current research interests include power system risk assessment, complex network, as well as electromagnetic effects.

Yan-zhao Xie (Senior Member, IEEE) was born in Henan, China, in 1973. He received the Ph.D. degree in electrical engineering from Tsinghua University, Beijing, China, in December, 2005. He is currently a Professor of School of Electrical Engineering, Xi'an Jiaotong University, China. His research interests include electromagnetic compatibility, electromagnetic transients in power system and high-power electromagnetics, etc. He has been the director of National Center for International Research on Transient Electromagnetics and Applications (TEA) since 2016.

Ning Dong was born in Henan, China, in 1995. She received the B.S. degree in electrical engineering from Xi'an Jiaotong University in 2016. She is currently working toward the Ph.D. degree in electrical engineering under the double degree program jointly supported by Xi'an Jiaotong University and Politecnico di Torino, Turin, Italy. Her current research interest includes numerical simulation of transient electromagnetic field.

Zong-yang Wang was born in Henan, China, in 1997. He received the B.S. degree in electrical engineering from North China Electric Power University, Beijing, China, in 2019. He is currently pursing the Ph.D. degree in electrical engineering with Xi'an Jiaotong University. His research interests include effect evaluation of high-power electromagnetics and geomagnetic storm.

Yi-fan Yang was born in Shanxi, China, in 1999. She received the B.S. degree in electrical engineering from North China Electric Power University, Baoding, China, in 2020. She is currently working toward the master's degree in electrical engineering with Xi'an Jiaotong University, Xi'an, China. Her research interests include electromagnetic compatibility and geomagnetic disturbance.